ELSEVIER

Materials Science and Engineering B97 (2003) 182–195

MATERIALS SCIENCE & ENGINEERING B

www.elsevier.com/locate/mseb

Review

Chemical and biological sensors based on optically confined birefringent chalcopyrite heterostructures

N. Dietz [a,b,*], F.L. Madarasz [a,c]

[a] *Xoetronics LLC, Ringoes, NJ 08551, USA*

[b] *Department of Physics and Astronomy, Georgia State University (GSU), University Plaza 29, Peachtree Center Avenue, Atlanta, GA 30303 3083, USA*

[c] *Center for Applied Optics, University of Alabama in Huntsville (UAH), Huntsville, AL 35899, USA*

Received 14 January 2002; received in revised form 3 July 2002; accepted 28 October 2002

Abstract

This paper introduces and discusses the design and application(s) of a new and unique integrated solid-state molecular sensor (SSMS) system. The SSMS is based on optically confined birefringent heterostructure technology, which has the capability of recognizing target chemicals and biological molecules in an ambient environment. The SSMS technology is applicable for miniaturized sensor devices that can be used for quick, remote screening and recognition of chemical hazards in the environment. For example, trace impurities related to air/water pollution can be continuously monitored. Just as important, however, the SSMS technology will have a worldwide impact—economically as well as technologically—when used in the detection of chemical and biological agents, as well as for a variety of medical sensing applications, such as to identify and monitor complex biological structures, test for allergic reactions and screen for common diseases. Moreover, it could hasten the time of development and introduction into the marketplace of critically needed new drugs by the monitoring of biochemical and molecular cellular responses to the candidate drugs. Materials selection criteria, growth parameters and device architecture requirements are given and discussed. In addition, the results of a recent phase matching calculation, substantiating the feasibility of the SSMS, are given and discussed. Published by Elsevier Science B.V.

Keywords: II–IV–V_2 chalcopyrites; Birefringent; NLO; Thin films; Heterostructures; Mixed-mode phase matching; Nonlinear coupled waveguides; Frequency agile laser; Molecular sensor; Chemical/biological agents

1. Introduction

The development of compact, highly integrated chemical and biological detection systems that for instance will provide accurate, continuous, real-time warnings prior to exposure to a chemical/biological (CB) hazard in the environment is of importance not only for chemical- (CW) but also biological weapons (BW) detection. In addition, it may be used for the monitoring of a variety of potential environmental air/water pollutants, as well as a variety of other CB monitoring applications. Presently, several optical detection concepts are being explored utilizing optical fibers and linear waveguided structures. A review of the various techniques has been provided by Boisdé et al. [1]. Each of the discussed techniques will have a niche market for a specific application. However, most of them lack the potential of further development due to limitations in either integration, handling or discrimination capabilities. The essential criteria that must be considered for the development of a compact, integrated CB detection system are summarized in Table 1.

There is a variety of applications where large volumes/distances are probed, which therefore, will follow different criteria as gleaned in Table 1. For instance, for the remote sensing of chemical agents, the integration criteria is of less importance compared with the efforts on developing high-intense, coherent laser light sources within the atmospheric infrared (IR) transparency window: mid-IR (3–5 μm) and far-IR (8–12 μm) [2–6]. The limitation given through the transparency

* Corresponding author. Tel.: +1-404-651-1427; fax: +1-404-651-2279.

E-mail address: ndietz@gsu.edu (N. Dietz).

0921-5107/02/$ - see front matter. Published by Elsevier Science B.V.
PII: S0921-5107(02)00436-1

Table 1
Criteria for a compact, integrated CB detection system

1	High sensitivity/detection limits
2	the capability to discriminate/identify known chemical and biological agents
3	the capability to identify potential harmful (comparison with known structures), but not yet identified chemical and biological agents
4	self-calibration and adjustable warning- and alarm level functions
5	robust maintenance and easy exchangeable modules
6	Operational at normal environmental conditions
7	minimal energy consumption
8	function reliability and life time, and
9	Portability

windows of the atmosphere and the requirement of high-power laser sources generates its own set of diagnostic techniques applied to a small but important group of environmental critical chemical agents. A locally applied CB sensor has the disadvantage of being able to probe only a limited volume but the advantage is, however, not being restricted to the atmospheric transparence window(s), which leaves the possibility of a wider detection range. In addition, the integration of remote read-out functions in such a locally deployed CB sensor unit may afford the opportunity to establish a wide-range CB monitoring network.

The focus of the present paper is to introduce and discuss the essential steps leading to this compact, highly integrated solid-state molecular sensor (SSMS) system, which are: the materials selection criteria, the growth parameters and the device architecture requirements. The SSMS is the subject matter of a recently awarded US patent and a pending patent continuation [7].

The SSMS is based on birefringent, optically confined nonlinear chalcopyrite (CP) heterostructures that can be operated as a tunable (frequency agile) IR laser source as well as an integral part of the CB detection system. Such a detection system has the advantage that it can utilize conventional, well-established semiconductor lasers that emit in the visible or near IR wavelength range with no cooling requirements. The useful transparency region of such a single- and multiple layered, nonlinear, waveguided CP heterostructure(s) extends from the near-IR up to far-IR wavelength regime depending on the CP compounds chosen. That is, from approximate ranges of 0.6–1 μm through 12–20 μm. The wavelength tunability in these CP heterostructures allows for the discrimination and identification of almost all molecular structures in a probed medium or attached at a probed interface/surface, using resonant phase- and/or amplitude sensitive detection. Fig. 1 illustrates the potential field of applications that can be exploited with optically confined birefringent heterostructures.

In Section 2 we outline the principle function and structure of a SSMS system, the monlithic integration of frequency agile laser light generation with sensor, detector- and electronic read-out elements as well as the availability of large-area, high-quality substrates. The most important criteria are the material selection for such a SSMS including materials integration and waveguiding aspect. These aspects are discussed in Section 3. Section 4 provides a brief introduction in the theory of nonlinear waveguide structures consisting of optical heterostructures based on CP thin films. Finally, in Section 5 we provide a summary.

2. Solid-state molecular sensor (SSMS)

A fully integrated SSMS structure is schematically depicted in Fig. 2. It consists of five basic elements labeled as such in the figure: (1) a laser light source; (2) a single or multiple optical confined CP heterostructure for the generation of coherent IR light (with either a broad IR wavelength output range or an externally controlled tuning range); (3) a sensor area where selected beam(s) interacts with an interface, a gas volume, or an ambient; (4) a detection unit(s); and (5) an analysis/discrimination unit with integrated feedback logic. Elements (2) and (3) can act collectively as a probe/sensor module. All of these components can be either monolithically integrated on one substrate, a hybrid-solution (for example micro-bonded heterostructures), or linked via optical connections (waveguides or optical fibers) to each other in close proximity. The central pieces of the SSMS are embedded birefringent CP heterostructures, which can be operated either as a tunable IR laser source, or as an integral part of the chemical agent detection system.

Element (2)—the 'wavelength tuning element' is a key feature of the SSMS device. It is built up of a birefringent CP layer(s) surrounded by optically confining and guiding cladding layers. A significant difference between the ordinary n_o and extraordinary n_e refractive indices of a birefringent CP layer enables the phase matching in the collinear propagation geometry (the most useful for various applications). For instance, if a CP layer is deposited such that the optical axis lies in the plane of the layer, the phase matching is obtained by properly choosing the angle between the optical axis and the propagation direction.

An understanding of physical principles underlying the nonlinear propagation of electromagnetic waves in optically confined single- and multiple- CP heterostructure(s) is essential for the construction of a realistic model to guide the growth, optimization, and fabrication of these heterostructures. The next step is the subsequent integration, evaluation and testing of each individual component specified in Fig. 2, leading to an integrated SSMS system.

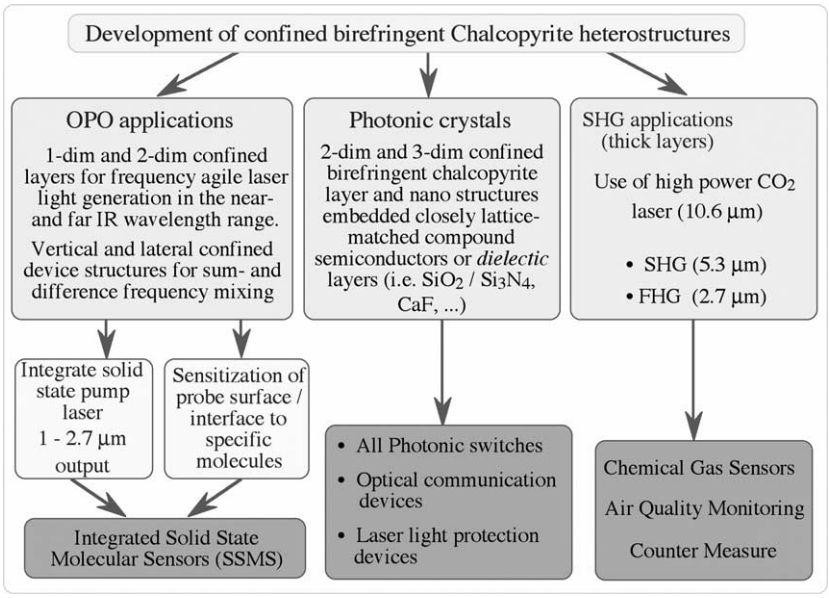

Fig. 1. Potential applications of optically confined birefringent CP heterostructures.

A theoretical analysis must address the following points: the simulation of wave propagation in birefringent waveguides and multiple coupled waveguided structures; the prediction of nonlinear optical (NLO) effects for coherent laser light generation via second harmonic generation (SHG), sum/difference frequency mixing, and optical parametric oscillator/amplifier (OPO/OPA) processes in such waveguided structures; and, the estimation of the electro–optic effect for frequency selection/adjustment. Also of importance is an understanding of how the propagating waves interact between adjacent layers. In particular, the modulation of wave propagation in the NLO layer via interaction with the waves in adjacent birefringent waveguides.

Fig. 3 schematically illustrates possible multiple layered constructs that can be utilized in a SSMS device. The frequency-agile optical parametric generator, based on graded nonlinear waveguide, is illustrated in Fig. 3a. All three participating waves propagate in spatially overlapping regions of the guide, which results in an efficient nonlinear interaction. Their cross extensions (in the growth direction) are schematically indicated as the transversal dimensions of the corresponding waves. Phase matching is achieved by the corresponding choice of the direction of the optical axis of the crystal relative to the propagation direction. A significant advantage is provided by the refractive index graded layers that permit waveguided propagation of the waves of different wavelengths in the same waveguide. In this manner, one has the flexibility to either have nonlinear generated waves propagate in the same spatial region as the pump wave or, if desired, to separate them and force them to propagate in different waveguides.

Wave propagation in the different waveguides is depicted in Fig. 3b. This shows an optical parametric generator based on a triple-waveguide structure with spatial separation of the pump, signal and idler waves. The three waveguides are single-mode, nonlinear, open resonators whose indices and thicknesses are chosen for the corresponding waves to propagate via the lowest modes. With the optical axis lying in the plane of the waveguide, phase matching is dependent on the angular orientation between it and the propagation vector of the wave. In addition, it is dependent on the orientation of

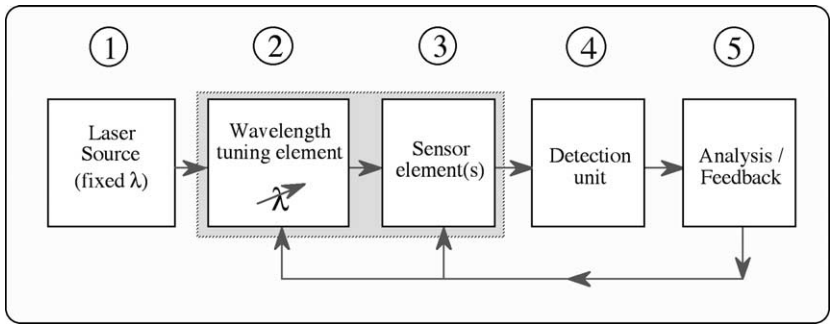

Fig. 2. Schematic of an integrated SSMS system.

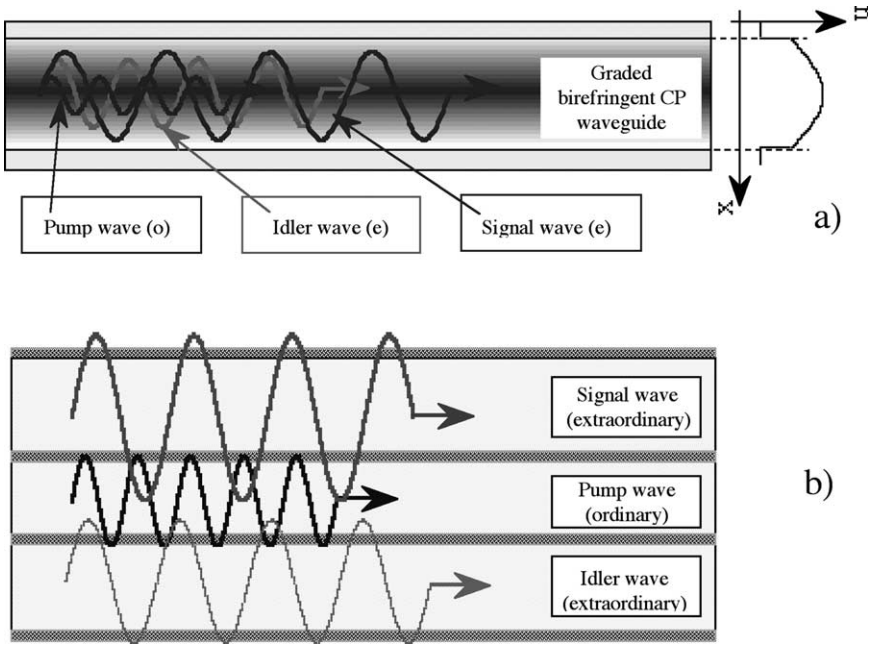

Fig. 3. Principle configurations: (a) an optical confined single CP structure, and (b) optical coupled, multiple CP heterostructures.

the polarization of the pump wave with respect to the axis of the guide.

That is, either transverse electric (TE) or transverse magnetic (TM), which governs the effective indices of refraction (See Section 4). Fig. 3b also illustrates the nonlinear interaction of the waves via the 'tunneling' between neighboring waveguides essentially, the overlapping of their evanescent waves. Phase matching and the strength of the interactions depend explicitly on the thickness and geometry of the guide(s). Moreover, this structure has the added flexibility that phase matched coupling can occur between the various modes of the guide, which is absent in bulk materials.

These configurations as those shown in Fig. 3 will add flexibility to the design, manufacturing and operation of the integrated sensors, parametric light sources (fixed-frequency and tunable) and frequency-agile lasers. The control in geometric wave propagation, the planar device design, and the engineering capabilities in the optical confinement of such CP heterostructures offer unique advantages that are absent in the bulk materials. The most evident are their mechanical robustness, small size, and weight. This makes them useful in airborne and portable devices.

Fig. 4 shows the details of potential device configurations for the elements (2) and (3) of the SSMS system introduced in Fig. 2. Here, the sensing element (3) follows sequentially the wavelength tuning element (2) as shown in Fig. 4a, and is constructed as a differential optical sensor. As illustrated in Fig. 4b and c, the upper-probing part-can be exploited for both, the probing of a gas volume, and the probing of attachments to surfaces/interfaces. By using partially reflecting side face, multiple internal reflectance conditions can be used to enhance the overall sensitivity of such a configuration. Such sensitivity enhancement schemes are important, for instance, to identify and analyze complex CB agents.

Further signal enhancement to specific agents is also possible with the SSMS structure. For example, electric field-modulation of either surface or interface structures are possible to either enhance or suppress the surface reactions of specific agents. Utilizing multiple, coupled waveguided structures will allow phase sensitive wave interference detection that may lead to an all-optical sensor system. Examples of achieving enhanced sensitivity are:

- electrical or magnetic biasing of active surface/interface for
  a) cleaning/reactivating of active surface,
  b) ionizing of molecules (enhancing of reactions),
  c) trapping of molecules;
- electrical field-modulation for either wavelength modulation or for phase sensitive detection.

Fields of applications include:

1) Sensors to identify and monitor complex biological structures.
2) Medical sensors to identify viruses and diseases.
3) Multi-area sensors for medical screening.
4) Compact multi-area sensors to monitor CB hazards in the environment.

Of particular interest is an all-optical sensing, discrimination and detection scheme as outlined in Fig. 5. It is based on the wave separation shown in Fig. 3b. The

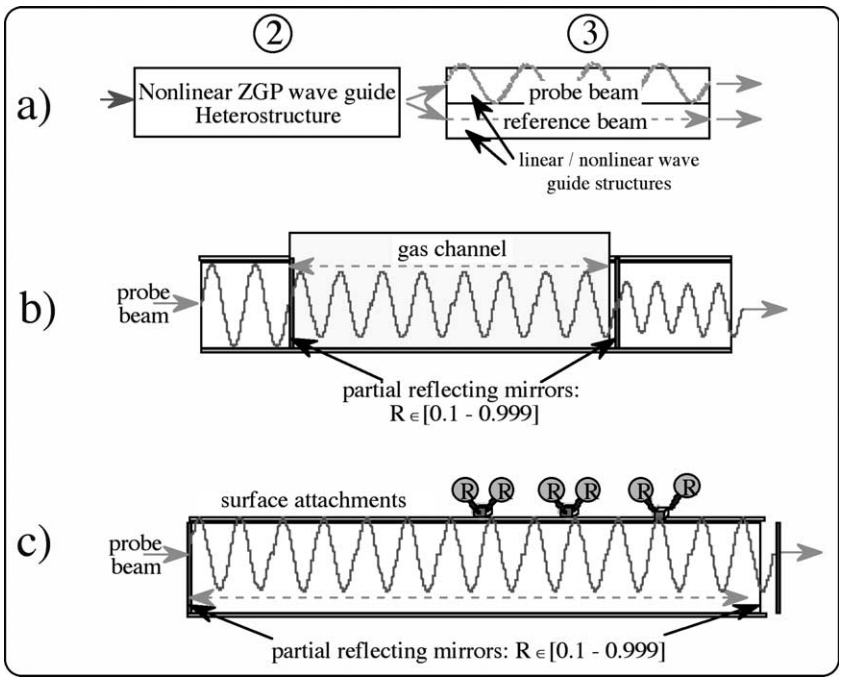

Fig. 4. Detail of elements (2) and (3) in Fig. 2. (a) Differential sensing using two linear wave guides; (b) and (c): two scenarios for probing a gas volume and for probing surface attachments, respectively.

SSMS sensing area consist of three interacting waves each predominantly propagating in a separate guide. As alluded to above, the spatial overlap of their evanescent waves penetrating into the adjacent guides gives rise to nonlinear interactions. Intuitively, it is expected that their interactions will be weak. However, this is compensated for by a high Q factor (low losses) of the waveguides. The principal advantage of this design is that the signal wave is separated from the pump and idler waves, which will dramatically decrease background scattering and noise. This is especially useful when using such devices as integrated sensors in the detection and discrimination of specific molecular targets. For such a use, the upper cladding in Fig. 5 should be chemically sensitized to allow absorption of specific, targeted molecules. Such a sensitized surface

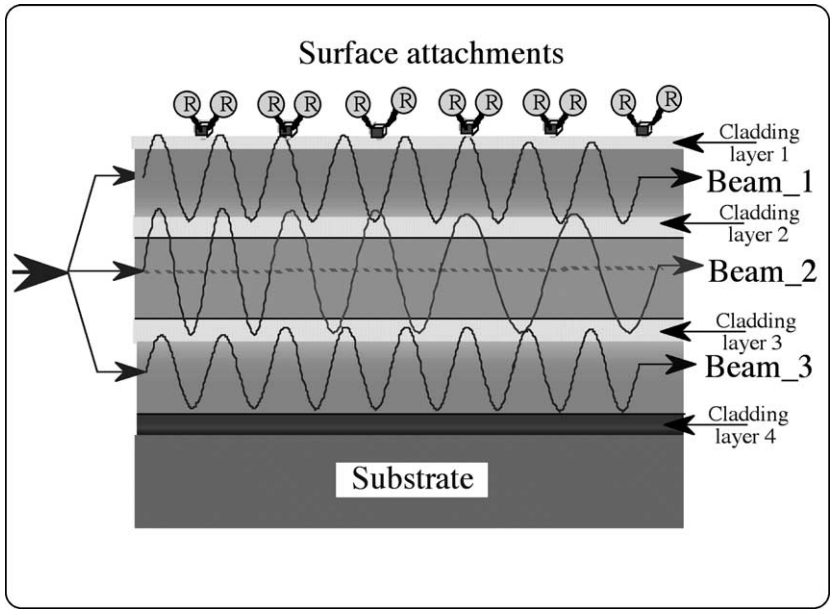

Fig. 5. Schematic of a differential sensor configuration using multiple layered linear/NLO confined heterostructures for high sensitive surface attachments characterization.

reaction layer will alter its optical dielectric properties upon reaction(s) with a specific molecule, antigen or antibody.

The alteration due to the absorbed molecules/structures will perturb the propagation condition of the signal wave and shift the OPO frequency. This frequency shift, though small, can be measured, e.g. by optical beats method that is based on coherency of the signal wave. Accounting for the dielectric properties of the adsorbent molecules will be made by considering them as a composite and using a well-developed method given in a paper by Stockman, et al. [8] The compact spatial integration capability of such a the SSMS system will foster the development of highly sensitive miniaturized sensor and multi-area sensors that will accelerate the detection of various biochemical and molecular species.

The development and optimization of optically confined birefringent CP heterostructures as well as the physical understanding of optical interactions in confined birefringent heterostructures and optically coupled multiple heterostructures, is of crucial importance for the SSMS development. Its successful development requires material selection and assessment, and the optimization of the structural, physical and NLO properties of the potential CP heterostructures. The next step requires the establishment of optical data bases containing spectral dependent absorption energies of CB agents (optical fingerprints), their optical absorption strengths and attachment probabilities on selected surfaces, and the design for optimum bonding and specificity of surfaces with regard to specific agents. These efforts are crucial to obtain:

a) the optical cross-sections and attachment factors,
b) the input parameters for the design and optimization of surface attachment layers,
c) an assessment of achievable and required device sensitivities,
d) the required input parameters for device design criteria.

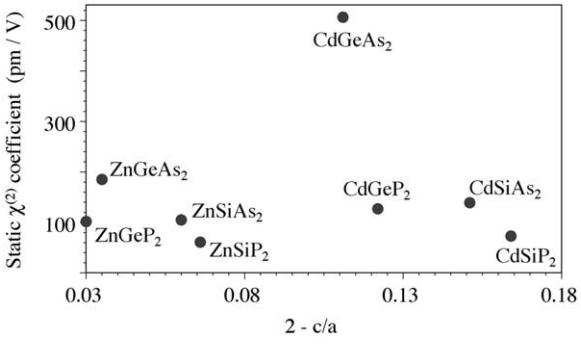

Fig. 6. NLO coefficients $\chi^{(2)}$ for the CP compounds $Cd(Ge_{1-x}Si_x)(As_{2-y}P_y)$ and $Zn(Ge_{1-x}Si_x)(As_{2-y}P_y)$.

In the following section we provide details of II–IV–V_2 CP materials and assess their particular usefulness and advantage(s) when used in an SSMS system. Specific attention is paid to materials properties needed for highly integrated optical diagnostic devices that are applicable to environmental sensors, biological diagnostic tools, and medical diagnostics devices.

3. Materials selection and materials integration considerations

3.1. Bulk and structural properties of III–IV–V_2 chalcopyrites

The potential of ternary III–IV–V_2 bulk CP compound semiconductor materials for NLO applications have been studies intensively during the last decades [9–12]. Although the CP semiconductors have electrical and optical properties comparable or superior to their group IV, III–V or II–VI counterparts, for many applications they have advantages due to their lower crystal symmetry. Being optically birefringent and pleochroic their optical and electro-optical properties are highly orientation dependent, thereby making them more sensitive to their environment. In principle, it enables new capabilities, especially in thin-film coupled-waveguide devices, where the possibility of controlling layer compositions, thicknesses, and spacings is expected to lead to new levels of performance in linear and nonlinear devices.

The highest nonlinear coefficients in the class of II–IV–V_2 semiconductors are reported for the compound systems $(Zn_{1-x}Cd_x)GeAs_2$, $Zn(Ge_{1-x}Si_x)As_2$ and $Zn(Ge_{1-x}Si_x)P_2$. As depicted in Fig. 6, all these systems have a positive birefringence. The associated second-order nonlinear susceptibility, $\chi^{(2)}$, increases correspondingly with the substitution of As for P, Ge for Si and Cd for Zn [11]. $CdGeAs_2$ is reported to have the highest NLO coefficient in the class of phase-matchable compounds [13]. Note that even the low lying compound $ZnGeP_2$ has a NLO coefficient approximately 160 times greater than KDP, making it one of the most efficient nonlinear crystal in the wavelength range 0.7–12 μm.

The II–IV–V_2 class of compound semiconductors, space group $I\bar{4}2d$, are the isoelectric analogs of the zincblende gallium phosphide (GaP), space group $F\bar{4}3m$, whereby, the average number of bonding electrons per atom remains unchanged. For this reason they are known as pseudo III–V compounds. The unit cells of the CP compounds $ZnGeP_2$ and $CdGeAs_2$, shown in Fig. 7, have a total of 16 atoms: four zinc (cadmium), four germanium and eight phosphorus (arsenide) atoms. The analogous zincblende structure of GaP is of a similar construction, but its unit cell has a total of eight

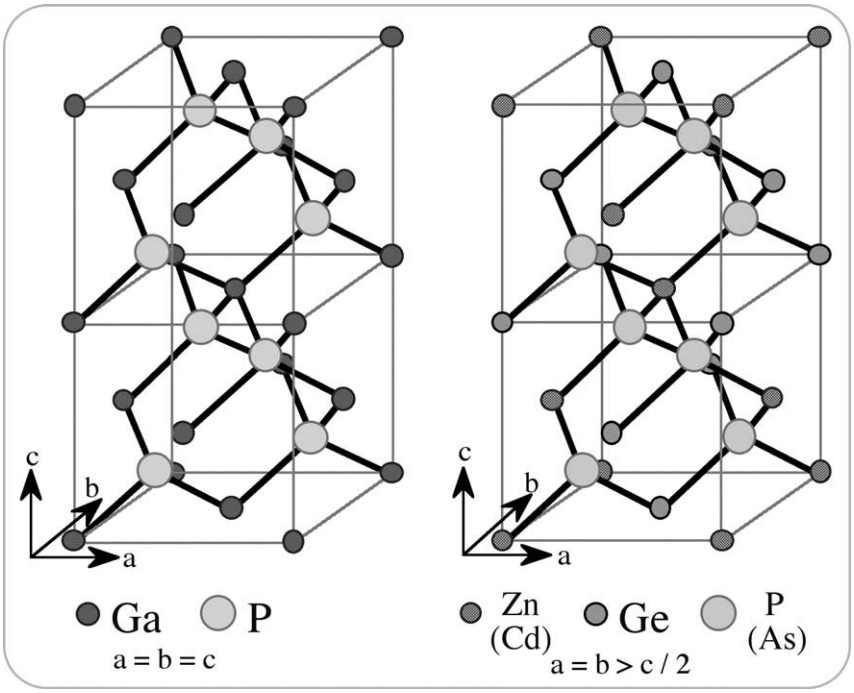

Fig. 7. Crystal structures for GaP (zincblende) and for $ZnGeP_2$/$CdGeAs_2$ (CP structure).

atoms (four cations and four anions) with equal a, b, c lattice parameters.

The ordered arrangement of the two cation species, tetrahedrally coordinated to the anion atoms, in CP unit cell leads to twice the c-axis height of the analogous zincblende cell. However, the differences in the two cationic species surrounding the anion and the manner of ordered substitution accounts for a peculiar distortion in the c-axis. $ZnGeP_2$ and $CdGeAs_2$, in which $a = b > c/2$, have slight compressions along the c-axis $a = 5.463$ Å, $c/a = 1.966$ [14] and $a = 5.943$ Å, $c/a = 1.888$ [14], respectively. These compressions have a pronounced effect on their observed nonlinear electrical and optical properties.

During the last 20 years significant progress has been made in optimizing the growth of $CdGeAs_2$ and $ZnGeP_2$ bulk crystals and in analyzing defect related properties in these materials. Further research will be required to understand, optimize and control the defect chemistry and surface-/interface properties in these materials. Critical issues that must still be addressed for the bulk materials are:

a) the control of the defect chemistry in growth processes;
b) n-type and/or p-type doping;
c) surface and/interface stabilization;
d) the NLO properties of quaternary systems.

For heteroepitaxial CP compound structures the critical issues to be addressed are:

a) evaluation and comparison of the defect chemistry of bulk materials with that of materials grown at lower temperatures by organometallic chemical vapor deposition (OMCVD) and liquid phase epitaxy (LPE),
b) improvement of bulk materials, for instance homoepitaxial overgrowth of CP surfaces and heteroepitaxy of layers for antireflection coatings, etc.,
c) device structures, for instance, p–n/n–p diode structures for detectors, guided layers as active NLO elements for frequency-agile light generation, etc.

3.2. Materials selection considerations for optical confined III–IV–V_2 CP heterostructures

The development of thin-film growth techniques for the CP materials is of critical importance not only to extend the unique nonlinear properties of bulk CP materials to a wider range of applications, but also improve the NLO properties of bulk materials and device structures. The focus here will be to consider CP materials requirements needed in the construction of a totally integrated solid state optical sensor system. Next to the availability of high-quality, lattice-matched substrates, the following selection criteria must be examined carefully:

a) nonlinear figure of merit,
b) a large, transparent wavelength range ($0.6 \leq \lambda \leq 20$ μm) for NLO interactions,

c) the availability of lattice-matched cladding layer to optically confine the CP heterostructures;
d) tuning of refractive indices in graded index CP heterostructures, cladding layers, and coupled, multiple heterostructures;
e) stringent control of composition, stoichiometry, point defect chemistry as well as extended defect formation and propagation are required for the fabrication of heterostructures with sufficiently good optical quality.

Fig. 8 summarizes the lattice constants and band gap energies of several CP materials, together with the lattice constants and band gap energies of potential group IV, III–V, and II–VI substrates. From this, it appears that lattice-matched growth conditions for achieving controlled stoichiometry in quaternary CP materials systems may be possible for four materials systems:

1) 1 $(Cd_{1-x}Zn_x)GeAs_2$ or $CdGe(As_{2-x}P_x)$ on InP substrates,
2) $Zn(Ge_{1-x}Si_x)As_2$ or ZnGe $(As_{2-x}P_x)$ on GaAs substrates, with lattice-matching cladding layers formed by compositionally controlled $GaAs_{1-x}Al_x$ layers,
3) $Zn(Ge_{1-x}Si_x)P_2$ on GaP, or Si substrates, with lattice-matching cladding layers made from compositionally controlled $GaP_{1-x}Al_x$ or $ZnS_{1-x}Se_x$ layers, and
4) $Zn(Ge_{1-x}Si_x)N_2$ on GaN substrates, with lattice-matching cladding layers made from compositionally controlled $Ga_{1-x}Al_xN$ and/or $Ga_{1-x}In_xN$ layers.

The lack of any lattice-matching and optically confining cladding materials for $(Cd_{1-x}Zn_x)GeAs_2$ or $CdGe(As_{2-x}P_x)$ compounds on InP will make these systems extremely difficulty to work with and to manufacture high quality multiple heterostrucutres. However, because of their high optical nonlinearities, these compounds may have potential applications in quantum confined NLO nanostructures and in strained layered heterojunction optical devices.

The nearly lattice-matched growth of $ZnGeAs_2$ on GaAs substrate by OMCVD has been investigated by Solomon et al. [15]. Their studies show that high-quality p-type $ZnGeAs_2$ layers can be grown on (100) GaAs. They did encounter problems with the formation of antiphase domain boundaries, the high solubility of Ge in these layers (stoichiometry control), and the growth on other than (100) GaAs surfaces [15,16]. Compared with the bulk crystal, *a* larger *c*/*a* ratio was observed, which may result in a reduction of birefringence in these layers. Unfortunately, no detailed information concerning the birefringent properties was given. There is, however, a continued and growing interest in this system. Soboley et al. [17] have investigated the electronic and optical properties above band gap ($E > E_g$) and correlated the data to theoretical band structure calculations. Most recently, theoretical studies on the structural and electronic properties of $ZnGeAs_2$ and $ZnGeAs_2$/GaAs superlattices have been done by Janotti et al. [18].

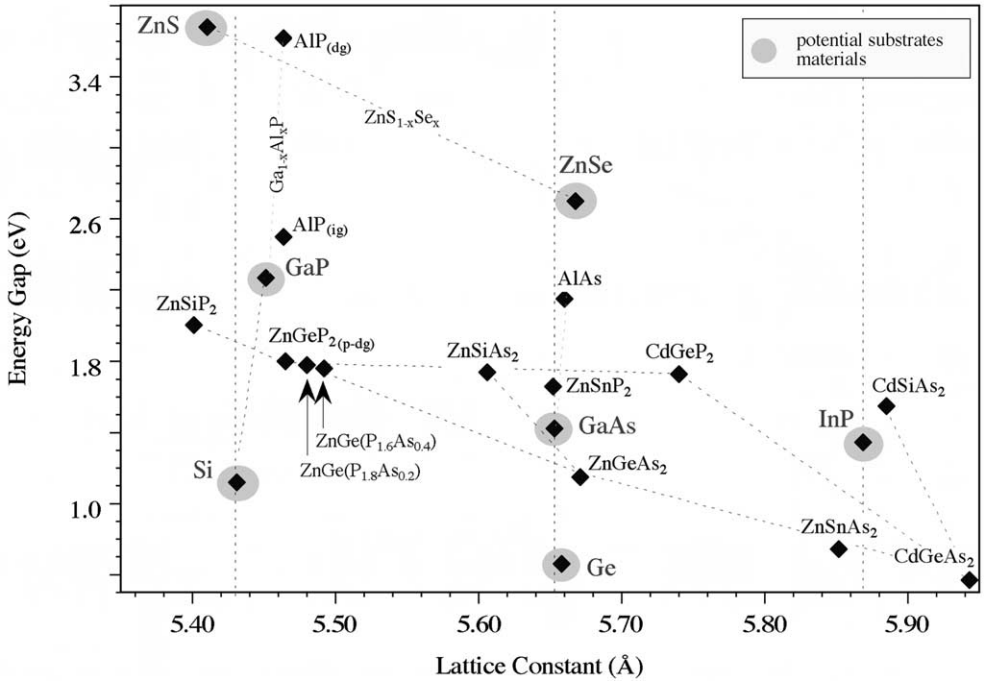

Fig. 8. Energy gaps and lattice constants for the selected III–IV–V_2 CP compounds in relation to group IV, III–V and II–VI semiconductors (dg: direct gap, ig: indiect gap, p-dg: pseudo-direct gap).

These studies show the persistent interest in this material system for photovoltaic and NLO applications.

The formation of operational NLO waveguided $ZnGeAs_2$ heterostructures clearly depends on the knowledge of the indices of refraction below the bandgap. However, precise values are presently undetermined. Fig. 9 shows the refractive index of Al_x-$Ga_{1-x}As$ as a function of excitations at energies lower than E_g for various compositions, x, of Al [19]. Superimposed on this plot are the ordinary, n_o, and extraordinary, n_e, indices of refraction of $ZnSiAs_2$, which is birefringent [20]. Also shown is the region of refractive indices for $ZnGeAs_2$, estimated from data given by Konstantinova et al. [21]. He reported a value of 12.3 for the high frequency dielectric constant, ε_∞, which corresponds to a refractive index of $n_\infty = 3.507$. If one considers this value together with the dependence of the refractive index on lattice-matched $Al_xGa_{1-x}As$ layers [19] depicted in Fig. 9, it suggests the possibility of optical confined $Al_xGa_{1-x}As/ZnGeAs_2/\ldots$ multiple heterostructures, with $ZnGeAs_2$ as an embedded, active birefringent layer.

The third system, $ZnGeP_2$–$ZnSiP_2$ on GaP, or Si substrates is of special interest. It combines a high NLO figure of merit with the availability of a lattice-matched optical confinement layers and the potential of integrated optoelectronic structures on Si substrates. The total variation of the a-axis lattice parameter at room temperature in the $ZnGeP_2$–$ZnSiP_2$ system ranges from 5.399 to 5.465 Å, and thus straddles the lattice constants of both GaP (5.4512 Å) and silicon (5.431 Å).

Refractive index values for the birefringent CP material system $Zn(Ge_{1-x}Si_x)P_2$ [20] and potential optical cladding materials GaP [22], AlP [23], $Ga_{1-x}Al_xP$ or ZnS [23] grown lattice-matched on GaP and/or Silicon substrates are show in Fig. 10. The lattice constant of $Ga_{1-x}Al_xP$ as a function of Al composition, x, varies from $a = 5.45120$ Å at $x = 0$ (GaP) to $a = 5.46350$ Å at $x = 1$ (AlP). Note that this is a lattice mismatch of only 0.2% over the entire composition range. The change in composition allows for the tuning of the refractive index of approximate 10% at 3 μm and 9% at 10 μm wavelength. With this, $Ga_{1-x}Al_xP$ is an ideal optical confinement layer for the higher indexed birefringent $ZnGeP_2$ or $Zn(Ge_{1-x}Si_x)P_2$ layer.

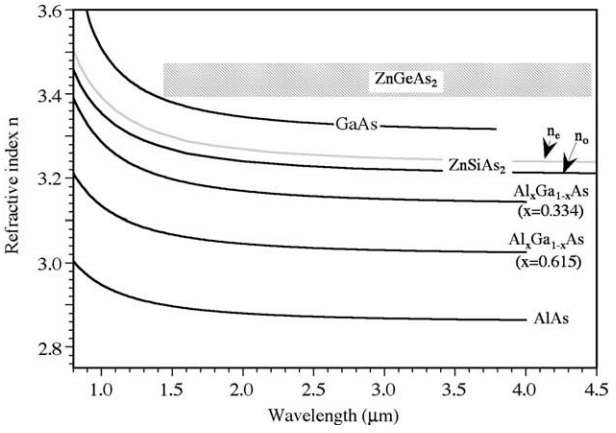

Fig. 9. Refractive index of $Al_xGa_{1-x}As$ below the band gap as a function of composition x [19], together with refractive index data for $Zn(Ge_{1-x}Si_x)As_2$.

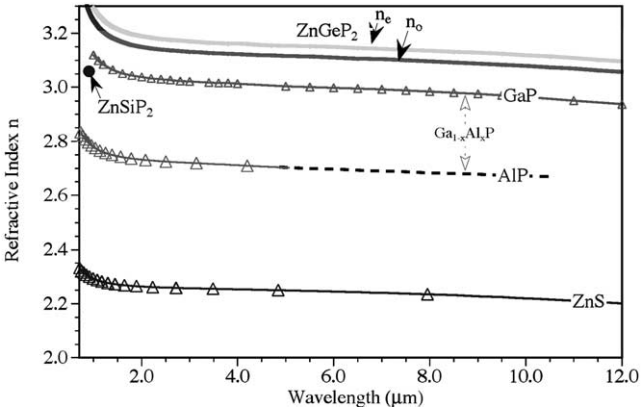

Fig. 10. Refractive index values for the birefringent CP material system $Zn(Ge_{1-x}Si_x)P_2$ and potential optical cladding materials.

Only two values of refractive indices have been reported [24] for $ZnSiP_2$: $n = 3.31$ at 600 nm and $n = 3.06$ at 900 nm. The direct energy gap in this compound was calculated at 2.98 eV, and modulated reflectance spectra on $ZnSiP_2$ show [25] the first direct transition occurs at 2.97 eV followed by another strong transition at 3.06 eV. These values correspond to electronic band transitions $(\Gamma_4, \Gamma_5) \rightarrow \Gamma_1$, respectively [25]. Electronic band structure calculations have been carried out by J.L. Shay et al. [25]; C.V. de Alvarez et al. [26]; J.E. Jaffe et al. [27]; A. Heinrich et al. [28]. The origin of experimentally observed transition [29] in $ZnSiP_2$ corresponding to an energy of 2.0 eV has not been explained to date.

Another cladding materials system is CaF_2. This system is also closely lattice-matched to Si at room temperature [30] ($a = 5.46306$ Å). Its epitaxial growth as lattice matched dielectric of silicon has been pioneered by Ishiwara and Asano[26]. CaF_2 provides for an even larger difference in refractive index [30], $n = 1.4288$–1.3989 over the range of 1–5 μm, respectively, and has a transparency region from 0.1 to 10 μm. In addition, it may serve as a better diffusion barrier than GaP and $Zn(Ge_{1-x}Si_x)P_2$. However, because of the large electronegativity of fluorine, significant differences are expected in the initial stages of the epitaxial growth when $ZnGeP_2$ is grown on CaF_2 coated with Si as opposed to when it is grown directly on CaF_2. The expected differences must be carefully studied experimentally.

Fig. 11 shows a bright field transmission electron micrograph (TEM) of a multiple GaP/$ZnGeP_2$ hetero-

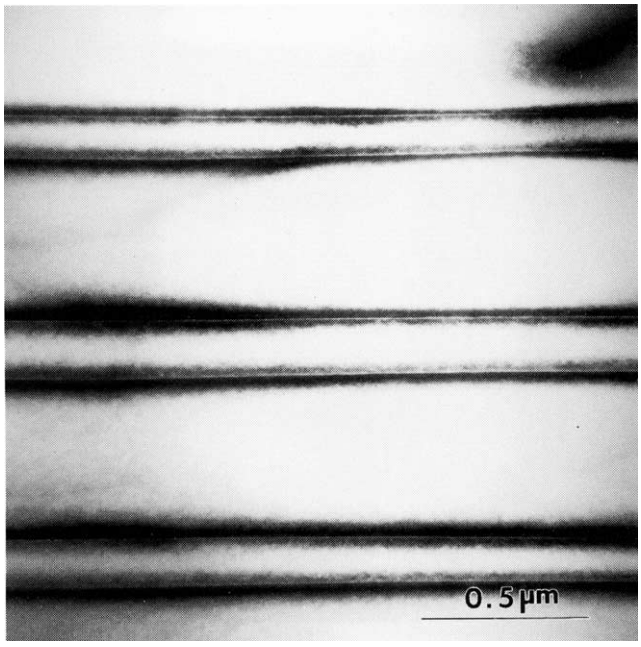

Fig. 11. Cross-sectional TEM bright field image of a multiple GaP/$ZnGeP_2$ heterostructure grown on a (001) GaP substrate [39].

structure grown on a (001) GaP substrate [31–37]. It is illustrative of the junction quality that may be achieved in growth. It also demonstrates the feasibility of manufacturing high-grade GaP–$Zn(Si_xGe_{1-x})P_2$, Si–$Zn(Si_xGe_{1-x})P_2$ single heterostructures and $Ga_{1-x}Al_xP$–$Zn(Si_xGe_{1-x})P_2$ multiple heterostructures which, in fact, were grown several years ago [31–37]. The growth of these heterostructures on (001) and (111) GaP and Si substrates was accomplished by OMCVD, utilizing dimethylzinc (DMZ), hydrogen diluted germane(0.33%), phosphine(10%) and disilane(0.2%) as source materials. At growth temperatures around 580 °C, high-quality epitaxial layers with mirror smooth surfaces were produced. TEM and secondary ion mass spectrometry (SIMS) of the GaP–$ZnGeP_2$–GaP multi-heterostructures showed sharp interfaces between the layers and high purity of the epilayers as compared with bulk $ZnGeP_2$ single crystals grown by directional solidification. The TEM and SIMS analysis also revealed the formation of extended defects, while electrical measurements revealed intrinsic point defects dominating p-type conductivity. Experience tells us that both can be minimized through a careful and refined materials development effort. These challenges become even more crucial in the quaternary $Zn(Si_xGe_{1-x})P_2$ system, which allows the growth of exact lattice matched heterostructures on silicon.

Recent advances in real-time monitoring and control of OMCVD processes [38] make it possible to control defect formations, their interactions and propagation during the later stages of heteroepitaxy growth. Defect formations are strongly coupled to the kinetics of heteroepitaxial growth. By virtue of this fact, they are closely related to surface structure that depends on both reconstruction and the nature and distribution of defects in the epitaxial film. So far, the progress in understanding and controlling thin film growth has been very slow, since little is known about chemical reaction pathways and reaction kinetics parameters during the decomposition process of the organometallic precursors.

Fig. 12 depicts schematically a planar nonlinear waveguided $Zn(Si_xGe_{1-x})P_2$ heterostructure, embedded in optically confined cladding layer, grown either on Si, GaP, and/or ZnS substrates. The choice of the substrate and the subsequent deposited layers have to be closely lattice matched and, at the same time, provide the proper refractive index to guide the waves in the above $Zn(Si_xGe_{1-x})P_2$ layer(s). Such optically confined birefringent layers offer advantages in tuning capability and phase matching, which can greatly enhance the operational characteristics of frequency-agile IR laser light generation. Potential combinations of closely lattice-matched heterostructures, capable to optically confine a birefringent $ZnGeP_2$ or $Zn(Si_xGe_{1-x})P_2$ active layer, are summarized in Table 2.

The availability of large high quality substrates along with lattice-matching considerations favors the use of Si-substrates. However, the growth on a GaP substrate has the advantage that its lower refractive index, compared with $ZnGeP_2$, acts at the same time as a cladding layer for the waveguide heterostructure. The engineering of optically abrupt or graded confinement structures can be achieved in compositional graded $Ga_{1-x}Al_xP$ layers with negligible lattice-mismatch within the heterostructures. To achieve optical confined heterostructures with larger differences in the refractive indices, the lattice-matched growth on a ZnS substrate is possible with $ZnS_{1-x}Se_x$ confined cladding layers. The feasibility of such heterostructures has to be explored experimentally.

4. Theoretical background

CP compound semiconductors are being used to achieve wavelength agility through much of the IR spectrum. However, many applications, such as OPO and SHG, are limited by the phase-matching requirements of the bulk material. For example, $ZnGeP_2$ would make an excellent frequency doubler of 10.6 μm radiation (yielding 5.3 μm radiation) but the phase matching conditions are difficult to achieve, which in turn places severe limitations on its conversion efficiency. The extraordinary wave index of refraction of $ZnGeP_2$ at 10.6 μm is almost exactly equal to the ordinary wave index of refraction at 5.3 μm making phase matching in bulk material marginal at best. This limitation, and corresponding limitations for other

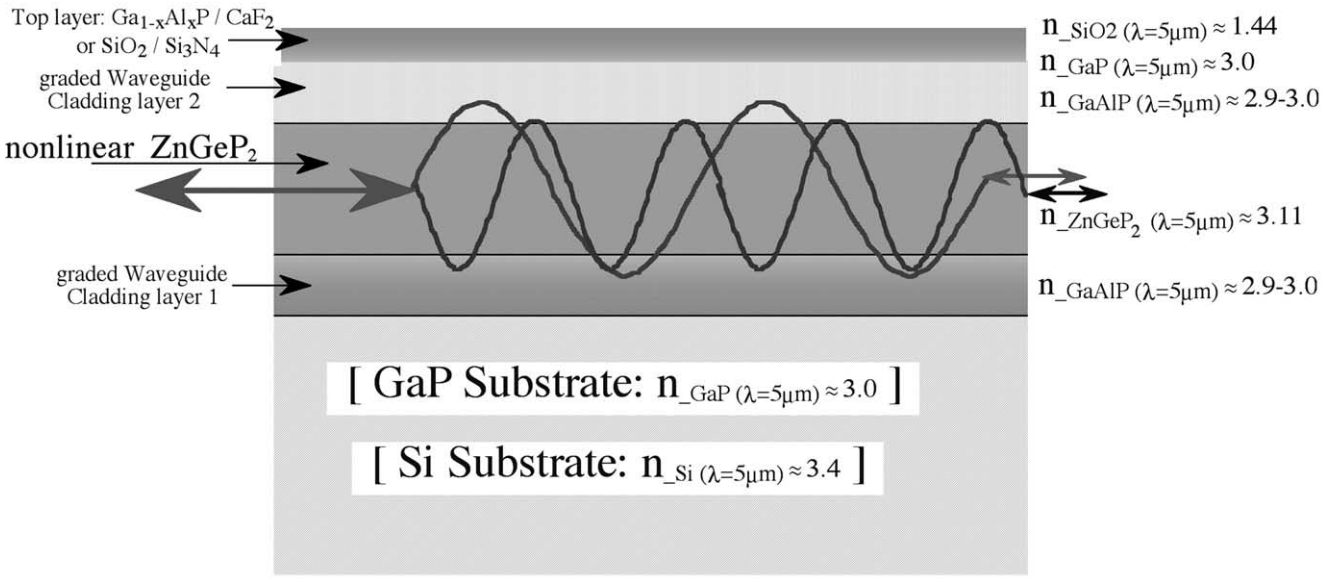

Fig. 12. Vertical schematic of layered multiple heterostructures, containing a birefringent waveguided layer embedded between two lower indexed cladding layers.

nonlinear processes, can be avoided by incorporating the $ZnGeP_2$, or other appropriate CP materials, in a waveguide structure. For example, the phase matching region for SHG can be considerably extended by coupling the pump into the guide in the fundamental, $m = 0$, mode and phase matching to the $m = 2$ mode of the second harmonic. In a recent paper [40], Dimmock et al. analyzed the phase matching conditions for SHG and OPO in birefringent nonlinear semiconductor waveguides and apply their results to the model system of $ZnGeP_2$ on a GaP substrate demonstrating the feasibility and efficient use of CP heterostrutures. In the remainder of this section we will outline their approach and results.

In order to achieve phase-matched conditions they considered that the optical axis of the $ZnGeP_2$ lies in the plane of the guide. In that case the angle between the direction of propagation of the wave in the guide and the optical axis of the guide material can be adjusted to achieve the phase matching condition. As shown below, they found that this can be accomplished for both SHG and OPO in $ZnGeP_2$ guides on GaP. Moreover, the waveguide geometry affords an additional opportunity for phase matching not available in bulk material. It is possible to couple radiation between different modes of the guide. They found that this can greatly extend the wavelength region over which phase-matched SHG can be achieved in a planar waveguide of $ZnGeP_2$.

If the optical axis of the, uniaxial, nonlinear guide material lies in the plane of the guide, optical propagation in the guide will be governed by two indices of refraction, one of which is dependent on the direction of propagation. If the wave is polarized perpendicular to the guide, TM mode, the index of the guide will be related to the ordinary index of the guide material. This index is independent of the direction of propagation and is referred to as n_{TM}. If the wave is polarized in the plane of the guide, TE mode, the index will depend on the

Table 2
Materials selection for optically confined $Zn(Ge_{1-x}Si_x)P_2$ layers

Number	Substrate	1 Cladding layer: Substrate ↔ waveguide	Active birefringent layer	2 Cladding layer: waveguide ↔ top
1	GaP	$Ga_{1-x}Al_xP$ ($x = 0$–0.5)	$ZnGeP_2$	$Ga_{1-x}Al_xP$ ($x = 0$–0.5) and thick GaP top layer
2	GaP	$Zn(Ge_{1-x}Si_x)P_2$ ($x = 0$–0.5)	$ZnGeP_2$	$Zn(Ge_{1-x}Si_x)P_2$ and thick GaP top layer
3	Silicon	$Zn(Ge_{1-x}Si_x)P_2$ (x = decreasing)	$ZnGeP_2$	$Zn(Ge_{1-x}Si_x)P_2$ and thick GaP top layer
4	Silicon	GaP followed by $Zn(Ge_{1-x}Si_x)P_2$ (x = decreasing)	$ZnGeP_2$	Graded $Zn(Ge_{1-x}Si_x)P_2$ layer with increasing x
5	Silicon	GaP followed by $Zn(Ge_{1-x}Si_x)P_2$ ($x = 0$–0.5)	$Zn(Ge_{1-x}Si_x)P_2$ fixed or graded composition	$Ga_{1-x}Al_xP$ ($x = 0$–0.2) and thick GaP top layer

direction of propagation with respect to the optical axis of the guide material. This index is referred to as n_{TE}.

Using the standard equations [41] for step index waveguides, n_{TM}, and n_{TE} are given by,

$$kt(n_O^2 - n_{TM}^2)^{1/2} = (m+1)\pi - \tan^{-1}\left(\frac{n_S^2(n_O^2 - n_{TM}^2)^{1/2}}{n_O^2(n_{TM}^2 - n_S^2)^{1/2}}\right) - \tan^{-1}\left(\frac{n_C^2(n_O^2 - n_{TM}^2)^{1/2}}{n_O^2(n_{TM}^2 - n_C^2)^{1/2}}\right), \quad (1)$$

$$kt(n^2 - n_{TE}^2)^{1/2} = (m+1)\pi - \tan^{-1}\left(\frac{(n^2 - n_{TE}^2)^{1/2}}{(n_{TE}^2 - n_S^2)^{1/2}}\right) - \tan^{-1}\left(\frac{(n^2 - n_{TE}^2)^{1/2}}{(n_{TE}^2 - n_C^2)^{1/2}}\right), \quad (2)$$

where

$$\left(\frac{1}{n}\right)^2 = \left(\frac{\cos\theta}{n_O}\right)^2 + \left(\frac{\sin\theta}{n_E}\right)^2, \quad (3)$$

n_O and n_E are the ordinary and extraordinary wave indices of the bulk guide material, n_S is the index of the substrate material, n_C is the index of the cladding, t is the guide thickness, $k = 2\pi/\lambda$ is the free space wave vector of the radiation, and m is the mode number for the wave in the guide. In addition, θ is the angle between the propagation direction and the optical axis of the guide material.

Using Eqs. (1)–(3) and a knowledge of n_O, and n_E, for the guide material, n_S for the substrate, n_C for the cladding as a function of wavelength, and choosing a value of guide thickness and propagation direction one can calculate the values of n_{TM}, and n_{TE} for the guide. These can then be used to obtain the phase matching conditions for the different nonlinear processes.

Dimmock et al. chose to examine the specific examples of OPO and SHG Type I phase matching in a $ZnGeP_2$ planar waveguide on a GaP substrate and with GaP cladding. The optical, or z-axis, of the $ZnGeP_2$ lies in the plane of the guide as does the x- (or y-) axis for the optimum Type 1 non-linear coupling. For SHG Type I phase matching they considered that the guide is pumped in the TE mode with propagation at an angle Θ with respect to the optical axis of the $ZnGeP_2$. Phase matching occurs for the angle Θ when

$$n_{TE}(2\lambda) = n_{TM}(\lambda) \quad \text{Type I, SHG.} \quad (4)$$

For OPO Type I phase matching they considered that the guide is pumped in the TM mode with propagation at a angle Θ with respect to the optical axis of the $ZnGeP_2$. Phase matching occurs for the angle Θ when:

$$\frac{1}{\lambda_P} = \frac{1}{\lambda_S} + \frac{1}{\lambda_I} \quad \text{Type I, OPO} \quad (5)$$

where λ_P is the wavelength of the pump, λ_S is the wavelength of the output signal, and λ_I is the wavelength of the idler wave, and:

$$\frac{n_{TM}(\lambda_P)}{\lambda_P} = \frac{n_{TE}(\lambda_S)}{\lambda_S} + \frac{n_{TE}(\lambda_I)}{\lambda_I} \quad \text{Type I, OPO.} \quad (6)$$

Using fits to the literature values [42] for the ordinary and extraordinary indices of bulk $ZnGeP_2$ [20] and GaP [6,20,22,43–45] and Eqs. (1)–(6) they calculated the phase matching angles shown in Fig. 13 for SHG and OPO for a 16 μm planar $ZnGeP_2$ guide on GaP operation in the $m = 0$ mode.

The corresponding phase matching angles for bulk $ZnGeP_2$ are shown for comparison. These results show phase matching angles for SHG quite similar to those of bulk $ZnGeP_2$ [46] as would be expected for a guide this thick. This simply shows that phase matched SHG and OPO should be readily obtainable in waveguides of $ZnGeP_2$ operating in the $m = 0$ mode. The applicability of the bulk indices for the waveguide will depend on the guide thickness, method of growth, degree of doping, lattice mismatch and internal strain. Bulk indices should be a good approximation for a well constructed 16 μm

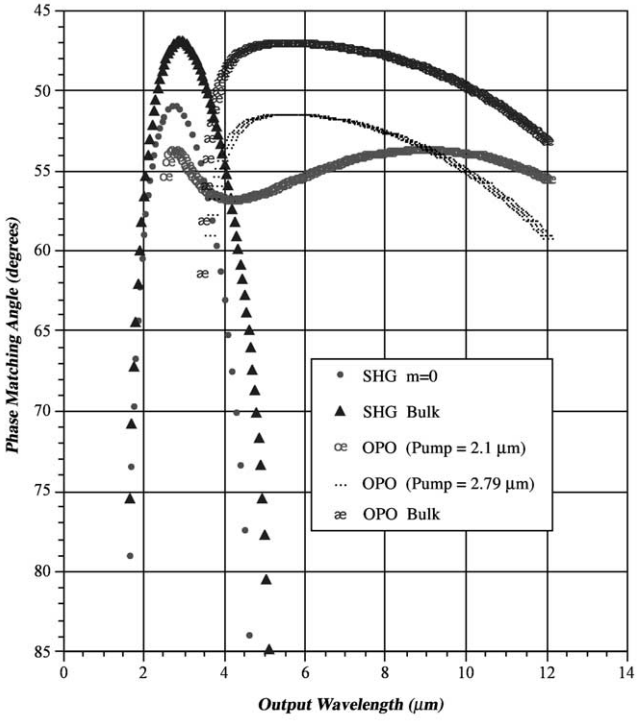

Fig. 13. Calculated phase matching angles for SHG and OPO in a 16 μm $ZnGeP_2$ waveguide with a GaP substrate and cladding layer compared with similar curves for bulk material.

thick guide with reasonable lattice match as could be obtained with $ZnGeP_2$ on GaP.

They also examined the case where coupling into the guide occurs in one mode of the guide, the nonlinear process within the guide couples energy to another mode and coupling out of the guide occurs from the second mode. Even though they did not do a detailed calculation of the strength of coupling, they estimated that nonlinear coupling from the $m=0$ to the $m=2$ mode, could be as large as 20% of the coupling to the $m=0$ mode of the guide for similar phase matching conditions. For the purpose of illustration, they considered the case of SHG where the input wave is in the $m=0$ mode with the second harmonic output considered in the $m=2$ mode. In this case, they used the value of n_{TM} (λ) for the $m=2$ mode but n_{TE} (2λ) for the $m=0$ mode. Their resulting phase matching angle is plotted in Fig. 14 along with the SHG curve from Fig. 13 and for the bulk material for comparison. Note that in this case phase matching for SHG can be obtained over wider wavelength region than for $m=0$ to $m=0$, or for bulk $ZnGeP_2$.

5. Summary

We introduced the design of a new and unique SSMS system that is based on optically confined, birefringent

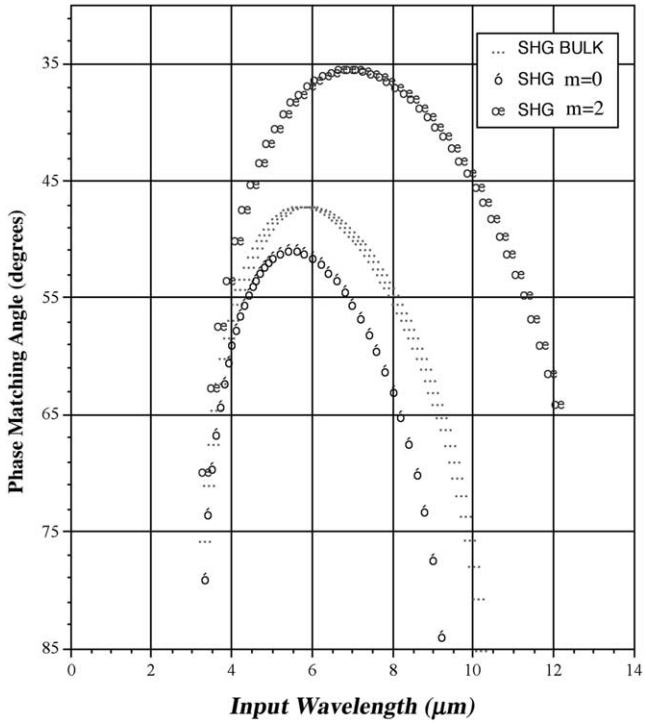

Fig. 14. Calculated phase matching angles for SHG in the 16 μm $ZnGeP_2$ waveguide of Fig. 13 pumped in the $m=0$ mode with output in the $m=2$ mode compared with the $m=0$ to $m=0$ coupling of Fig. 13 and that of the bulk material.

II–IV–V_2 compound semiconductor technology. Its application targets the recognition of chemicals and biological molecules in an ambient environment. Sensing and discrimination of chemical agents is achieved by monitoring and analyzing the NLO interactions in optically confined II–IV–V_2 heterostructures and the probing of linear/NLO evanesce wave coupling of interface with attached agents. We identified two II–IV–V_2 CP materials systems, $Zn(Ge_{1-x}Si_x)As_2$ and $Zn(Ge_{1-x}Si_x)P_2$, that are suitable for such a SSMS system. Both systems will allow for the construction of optically confined birefringent heterostructures, closely lattice-matched onto readily available group IV, III–V or II–VI substrates. Waveguided birefringent heterostructures based on the $Zn(Ge_{1-x}Si_x)As_2$ system will have the potential advantage of a monolithic integrated all optical sensor. At present, however, little is know about the linear and NLO properties of this material system. This aspect, together with optoelectronic integration aspects favors at present the development of optically confined birefringent $Zn(Ge_{1-x}Si_x)P_2$ layers on GaP and silicon substrates. This material system is also favored because of its larger optical transparency window.

The growth of such structures can be accomplished by OMCVD, which is particularly suited for II–IV–V_2 epitaxy, because of access to well developed source vapor compounds for this class of materials, and for nearly lattice matched III–V compounds, serving as substrates and confinement layers in multiple heterostructures. A combination of OMCVD and LPE might be suitable for thicker optical confined birefringent layers. Challenges that must be met in the development of such heterostructures are the optimization of the growth processes, the control of point defect chemistry, extended defects, carrier concentration and scattering by extended defects.

The theoretical analysis of phase matching in these nonlinear, birefringent heterostructures has been applied to the specific guide material $ZnGeP_2$ on a GaP substrate. The results showed that this structure has the added flexibility that phase matched coupling can occur between the various modes of the guide. Moreover, the coupling is a function of the guide thickness. These added degrees of freedom will allow for high gain under conditions where it is difficult or impossible to achieve in bulk material. The results also indicate, among other things, that $ZnGeP_2$ waveguides with harmonic output in the $m=2$ mode can be used for efficient SHG from input radiation around 10.6 μm where bulk efficiencies in this wavelength range are too small to be useful. Indeed, the realization of such a structure would pave the way for a myriad of novel opto-electronic devices.

References

[1] Chemical and Biochemical Sensing with Optical Fibers and Waveguides, G. Boisdé, A. Harmer (Ed.), ISBN 0-89006-737-6; Artech House, Inc., Norwood, MA 02062 (1996).

[2] P.A. Budni, K. Ezzo, P.G. Schunemann, S. Minnigh, J.C. McCarthy, T.M. Pollak, 2.8 micron pumped optical parametric oscillation in $ZnGeP_2$, OSA Proceedings on Advanced Solid-State Lasers, vol. 10, Proceedings of the Topical Meeting, 1991, pp. 335–338.

[3] P.A. Budni, P.G. Schunemann, M.G. Knights, T.M. Pollak, E.P. Chicklis, Efficient, high average power optical parametric oscillator using $ZnGeP_2$, OSA Proceedings on Advanced Solid-State Lasers, vol. 13, Proceedings of the Topical Meeting, 1992, pp. 380–383.

[4] Y.M. Andreev, P.P. Geiko, G.M. Krekov, O.A. Romanovskii, Detection of trace concentration of some simple pollutants in Tomsk, Proceedings of the SPIE-The International Society for Optical Engineering 1811, 1992, pp. 367–370.

[5] K. Stoll, J.-J. Zondy, O. Acef, Optics Lett. 22 (1997) 1302–1304.

[6] N.P. Barnes, K.E. Murray, M.G. Jani, P.G. Schunemann, T.M. Pollak, J. Opt. Soc. Am. B 15 (1) (1998) 232–238.

[7] N. Dietz, K.J. Bachmann, Chalcopyrite Based Nonlinear Waveguided Heterostructure Devices and Fabrication and Operating Methods, US Patent Number 6,442,319, issued August 27, 2002; and its continuation-in-part US Patent Application Serial No. 10/228,777, N. Dietz, F.L. Madarasz, filed August 25, 2002.

[8] M.I. Stockman, K.B. Kurlayev, T.F. George, Phys. Rev. B 60 (24) (1999) 17071–17083.

[9] J.L. Shay, J.H. Wernick, Ternary Chalcopyrite Semiconductors: Growth, Electronic Properties, and Applications, Pergamon Press, Oxford, New York, 1975.

[10] M.M. Tilleman, A Englander, Optical Eng. 39 (3) (2000) 758–762.

[11] S.N. Rashkeev, S. Limpijumnong, W.R.L. Lambrecht, Phys. Rev. B 59 (2) (1999) 2737–2748.

[12] K.L. Vodopyanov, F. Ganikhanov, J.P. Maffetone, I. Zwieback, W. Ruderman, Optics Lett. 25 (11) (2000) 841–843.

[13] V.G. Dmitriev, G.G. Gurzadyan, D.N. Nikogosyan, in: A.L. Schawlow, K. Shimoda, A.E. Siegman, T. Tamir (Eds.), Handbook of Nonlinear Optical Crystals, Springer Series in Optical Sciences, second ed (ISBN 3-540-61275-0), 1997, p. 64.

[14] O. Madelung, Semiconductor Physics; Basic Data of Semiconductors, second ed (ISBN 3540608834), Springer, 1996.

[15] G.S. Solomon, M.L. Timmons, J.B. Posthill, J. Appl. Phys. 65 (5) (1989) 1952–1956.

[16] G.S. Solomon, J.B. Posthill, M.L. Timmons, Appl. Phys. Lett. 55 (15) (1989) 1531–1533.

[17] V.V. Sobolev, S.P. Batanov, V.E. Grachev, Optics Spectrosc. 83 (1) (1997) 101–104.

[18] A. Janotti, Su-Huai Wei, S.B. Zhang, Sarah Kurtz, Phys. Rev. B 63 (2001) 195210–195217.

[19] S. Gehrsitz, F.K. Reinhart, C. Gourgon, N. Herres, A. Vonlanthen, H. Sigg, J. Appl. Phys. 87 (11) (2000) 7825–7837.

[20] G.D. Boyd, E. Buehler, F.G. Storz, Appl. Phys. Lett. 18 (1971) 301–304.

[21] N.N. Konstantinova, Yu V. Rud, M.A. Tairov, Sov. Phys. Semicond. 22 (9) (1988) 999–1001.

[22] A. Borghesi, G. Guizzetti, in: E.D. Palik (Ed.), Handbook of Optical Constants, Academic Press, 1985, p. 445.

[23] A.N. Pikhtin, A.D. Yas'kov, Sov. Phys.-Semiconductors 12 (6) (1978) 622–626.

[24] H. Bondriot, B. Foeller, H.A. Schneider, Phys. Status Solidi (a) 30 (1975) K121.

[25] J.L. Shay, B. Tell, E. Buehler, J.H. Wernick, Phys. Rev. Lett. 30 (20) (1973) 983–986.

[26] C.V. de Alvarez, M.L. Cohen, Phys. Rev. Lett. 30 (20) (1973) 979–9822.

[27] J.E. Jaffe, A. Zunger, Phys. Rev. B 30 (2) (1984) 741–756.

[28] A. Heinrich, W. Cordts, J. Monecke, Phys. Stat. Sol. (b) 107 (1981) 319–333.

[29] I.S. Gorban, V.A. Gorynya, V.I. Lugovoi, I.I. Tychina, Sov. Phys. Solid State 16 (1974) 1029–1030.

[30] D.F. Bezuidenhout, in: E.D. Palik (Ed.), Handbook of Optical Constants of Solids II, Academic Press, Washington, DC, 1998, pp. 815–835.

[31] G.C. Xing, K.J. Bachmann, G.S. Solomon, J.B. Posthill, M.L. Timmons, J. Cryst. Growth 94 (1989) 381.

[32] G.C. Xing, K.J. Bachmann, J.B. Posthill, G.S. Solomon, M.L. Timmons, in: A.T. Macrander, T.J. Drummond (Eds.), Heteroepitaxial Approaches in Semiconductors: Lattice Mismatch and its Consequences, The Electrochemical Society, Pennington, NJ, 1989, p. 132.

[33] J.B. Posthill, G.C. Xing, G.S. Solomon, K.J. Bachmann, M.L. Timmons, 'Phase Identification and Defect Structures in II–IV–V_2 Heteroepitaxial Thin Films Grown on III–V Substrates,' Proceedings 47th Annual Meeting of the Electron Microscopy Society of America, 1989, pp. 582.

[34] J.B. Posthill, R.P. Burns, R.A. Rudder, Y.H. Lee, R.J. Markunas, K.J. Bachmann, 'Electron Microscopic Characterization of Diamond Thin Films and Substrates for Diamond Heteroepitaxial Growth,' Proceedings 47th Annual Meeting of the Electron Microscopy Society of America, 1989, pp. 561.

[35] G.C. Xing, K.J. Bachmann, J.B. Posthill, M.L. Timmons, in: J.T. Glass, R. Messier, N. Fujimori (Eds.), $ZnGeP_2$: A wide Bandgap Semiconductor for non-Linear Optical Applications, in Diamond, Boron Nitride, Silicon Carbide and Related Wide Gap Compound Semiconductors, Materials Research Society, Pittsburgh, PA, 1990, p. 615.

[36] G.C. Xing, K.J. Bachmann, J.B. Posthill, M.L. Timmons, J. Appl. Phys. 69 (1991) 4286.

[37] G.C. Xing, K.J. Bachmann, J.B. Posthill, M.L. Timmons, J. Cryst. Growth 113 (1991) 113–119.

[38] D.E. Aspnes, N. Dietz, Appl. Surf. Sci. 130–132 (1998) 367–376.

[39] G.C. Xing, K.J. Bachmann, J. Crystal Growth 147 (1/2) (1995) 35–38.

[40] J.O. Dimmock, F.L. Madarasz, N. Dietz, K.J. Bachmann, Appl. Optics 40 (9) (2001) 1438–1441.

[41] R.G. Huntsperger, Integrated Optics: Theory and Technology, second ed (chapter 2), Springer, New York, 1984.

[42] F.L. Madarasz, J.O. Dimmock, N. Dietz, K.J. Bachmann, J. Appl. Phys. 87 (3) (2000) 1564–1565.

[43] K. Kato, Appl. Optics 36 (12) (1997) 2506–2510.

[44] D.W. Fischer, M.C. Ohmer, J. Appl. Phys. 81 (1) (1997) 425–431.

[45] G. Ghosh, Appl. Optics 37 (1998) 1205–1212.

[46] M.C. Ohmer, R. Pandey (Eds.), 'Emergence of chalcopyrites as nonlinear optical materials', Materials Research Bulletin, Special Issue (July 1998).